Dressed bound states at chiral exceptional points

Yuwei Lu
School of Physics and Optoelectronic Engineering, Foshan University, Foshan 528000, China
and School of Physics and Optoelectronics, South China University of Technology, Guangzhou 510641, China

Haishu Tan*
School of Physics and Optoelectronic Engineering, Foshan University, Foshan 528000, China

Zeyang Liao†
State Key Laboratory of Optoelectronic Materials and Technologies, School of Physics, Sun Yat-sen University, Guangzhou 510275, China

(Received 17 January 2023; revised 11 April 2023; accepted 17 April 2023; published 27 April 2023)

Atom-photon dressed states are a basic concept of quantum optics. Here, we demonstrate that the non-Hermiticity of an open cavity can be harnessed to form the dressed bound states (DBSs) and identify two types of DBSs, the vacancylike DBS and Friedrich-Wintgen DBS, in a microring resonator operating at a chiral exceptional point. With the analytical DBS conditions, we show that the vacancylike DBS occurs when an atom couples to the standing-wave mode that is a node of the photonic wave function and characterized by null spectral density at cavity resonance. However, the Friedrich-Wintgen DBS can be accessed by continuously tuning the system parameters, such as the atom-photon detuning, and evidenced by a vanishing Rabi peak in the emission spectrum, an unusual feature in the strong-coupling anticrossing. We also demonstrate the quantum-optics applications of the proposed DBSs. Our work exhibits quantum state control through non-Hermiticity of open quantum system and presents a clear physical picture of DBSs at chiral exceptional points, which holds great potential for building high-performance quantum devices for sensing, photon storage, and nonclassical light generation.

DOI: 10.1103/PhysRevA.107.043714

I. INTRODUCTION

Dressed states are a hallmark of strong atom-photon interaction [1] and provide a basis for coherent control of quantum states, giving rise to a rich variety of important technologies and applications, such as quantum sensing [2], entanglement transport [3,4], photon blockade for quantum light generation [5–7], and the many-body interaction for scalable quantum computing and quantum information processing [8,9]. Dressed states with slow decay, i.e., a narrow linewidth, are appealing in practical applications. Although the linewidth of dressed states is the average of atomic and photonic components, it is often limited by the latter since the linewidth of the quantum emitter (QE) is much smaller than the cavity in a cryogenic environment. Therefore, a natural approach to reduce the linewidth of dressed states is by means of a high-Q cavity, which, however, is often at the price of a large mode volume [10,11] or requires elaborate design [12–14]. Furthermore, light trapping and release are time-reversal processes in linear time-invariant systems; thus, a cavity with high Q in general leads to low excitation efficiency, which is undesirable in practical applications. These disadvantages stimulate the exploration of alternative schemes to suppress the decay of dressed states.

Although leakage is inevitable for optical resonators, it also opens up new avenues for manipulating light-matter interaction by exploiting the non-Hermitian degeneracies [15,16], known as exceptional points. The presence of exceptional points renders exotic features of the system dynamics due to the reduced dimensionality of the underlying state space at exceptional points [17–19]. Particularly, previous studies have shown that the coalescence of counterclockwise (CCW) and clockwise (CW) modes in a whispering-gallery-mode (WGM) microcavity gives rise to a special type of exceptional point, called chiral exceptional points (CEPs) [20,21], which exhibit an unprecedented degree of freedom in state control, such as quantum and optical states with chirality [17,20,22] and the spontaneous emission enhancement associated with the squared Lorentzian response [18,23–25].

In this work, we propose and identify the formation of dressed bound states (DBSs) in an open microring resonator with CEPs, which we call a CEP cavity hereafter. A theoretical framework is established to unveil the origin and derive the analytical conditions of DBSs. We show that DBSs in the CEP cavity can be classified into two types, the vacancylike DBS [26] and the Friedrich-Wintgen DBS [6,27–29]. The vacancylike DBS has a unique feature in which its condition is irrespective of atom-photon coupling strength since the cavity mode the atom couples to is a node of the photonic

*Corresponding author: tanhaishu@fosu.edu.cn
†Corresponding author: liaozy7@mail.sysu.edu.cn

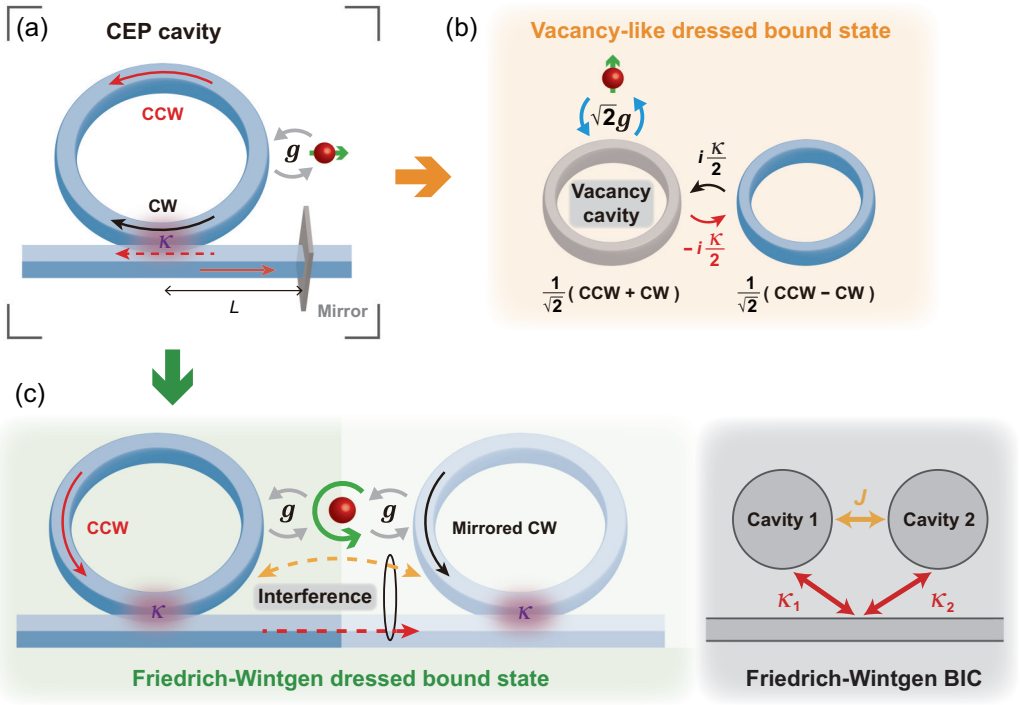

FIG. 1. (a) Schematic of the CEP cavity with a WGM microring coupled to a QE and a waveguide with a mirror at the right end. (b) Illustration of the origin of the vacancylike DBS: the standing-wave mode the QE coupled to is a node of a wave function. (c) Left: Illustration of the formation of the Friedrich-Wintgen DBS via the destructive interference of two coupling pathways between the CW and CCW modes. The CW mode is flipped to a CCW mode via mirror symmetry. Accordingly, the linearly polarized QE becomes circularly polarized. Right: Schematic diagram of the Friedrich-Wintgen BIC for two cavities.

wave function. By contrast, DBSs with a Friedrich-Wintgen origin depend on the system parameters, such as the frequency detuning and the coupling strength between different system components, which are required to fulfill the condition of destructive interference between two coupling pathways. We also discuss the characteristics of the spontaneous emission (SE) spectrum and dynamics associated with DBSs and demonstrate the corresponding quantum-optics applications.

II. RESULTS AND DISCUSSION

A. Model and theory

The CEP cavity we study is depicted in Fig. 1(a), where a WGM microring resonator is coupled to a semi-infinite waveguide with a perfect mirror (i.e., unity reflectivity) at the end. The mirror results in chiral coupling from the CCW mode to the CW mode and creates a CEP [23]. A linearly polarized QE couples to the CEP cavity with coupling strength g. We assume that the QE is embedded inside the cavity; thus, its coupling to free space via modes other than cavity modes is suppressed. Furthermore, although the CEP cavity supports a series of WGM resonances, here, we consider only a pair of degenerate CW and CCW modes. This is justified since in a realistic CEP cavity, the linewidth of the QE can be much smaller than the frequency spacing Δf between the adjacent WGM resonances. For example, Δf is evaluated as $\sim$11 THz for a SiN microdisk with a 2 μm radius [30,31], while the linewidth of CdSe/ZnSe quantum dots is approximately $\sim$1 THz at 77 K [32,33].

The quantum dynamics of the cavity QED system is described by the extended cascaded quantum master equation (see Refs. [34,35] and also Appendix. A for a detailed derivation)

$$\frac{d}{dt}\rho = -i[H,\rho] + \kappa\mathcal{L}[c_{\rm ccw}]\rho + \kappa\mathcal{L}[c_{\rm cw}]\rho + \kappa(e^{i\phi}[c_{\rm ccw}\rho, c_{\rm cw}^\dagger] + e^{-i\phi}[c_{\rm cw}, \rho c_{\rm ccw}^\dagger]), \quad (1)$$

where $\mathcal{L}[O]\rho = O\rho O^\dagger - \{O^\dagger O,\rho\}/2$ is the Liouvillian superoperator for dissipation of operator O. The Hamiltonian is given by $H = H_0 + H_I$, where the free Hamiltonian H_0 and the interaction Hamiltonian H_I read

$$H_0 = \omega_0\sigma_+\sigma_- + \omega_c c_{\rm ccw}^\dagger c_{\rm ccw} + \omega_c c_{\rm cw}^\dagger c_{\rm cw}, \quad (2)$$

$$H_I = g(c_{\rm ccw}^\dagger\sigma_- + \sigma_+ c_{\rm ccw}) + g(c_{\rm cw}^\dagger\sigma_- + \sigma_+ c_{\rm cw}), \quad (3)$$

where σ_- is the lowering operator of QE and $c_{\rm ccw}$ ($c_{\rm cw}$) is the bosonic annihilation operator for the CCW (CW) mode. ω_0 and ω_c are the transition frequency of the QE and the resonance frequency of cavity modes, respectively. The second line of Eq. (1) describes the chiral coupling in which the CW mode is driven by the output field from the CCW mode, where $\phi = 2\beta L$ is the accumulated phase factor of light propagation, with β and L being the propagation constant of the waveguide and the distance between the waveguide-resonator junction and the mirror, respectively. κ is the evanescent coupling of the cavity modes to the waveguide, which can be tuned by adjusting the cavity-waveguide separation. In order to achieve

effective coupling of CW and CCW modes, we consider the case in which κ is much larger than the intrinsic decay of the cavity, and thus, the latter is omitted in Eq. (1).

We consider the SE process in which there is at most one photon in the system and the case of resonant QE-cavity coupling ($\omega_0 = \omega_c$). The equations of motion in the single-excitation subspace can be obtained from Eq. (1),

$$\frac{d}{dt}\vec{p} = -i\mathbf{M}_c\vec{p}, \tag{4}$$

with $\vec{p} = [\langle\sigma_-\rangle, \langle c_{\rm ccw}\rangle, \langle c_{\rm cw}\rangle]^T$ and the matrix $\mathbf{M}_c$ being

$$\mathbf{M}_c = \begin{bmatrix} \omega_c & g & g \\ g & \omega_c - i\frac{\kappa}{2} & 0 \\ g & -i\kappa e^{i\phi} & \omega_c - i\frac{\kappa}{2} \end{bmatrix}. \tag{5}$$

The emission spectrum is experimentally relevant and also critical for understanding the quantum dynamics of a QE. Therefore, we investigate the spectrum properties of DBSs via the SE spectrum of the QE, which can be measured via fluorescence of the QE and is defined as $S(\omega) = \lim_{t\to\infty} \mathrm{Re}[\int_0^\infty d\tau \langle\sigma_+(t+\tau)\sigma_-(t)\rangle e^{i\omega\tau}]$ [1,36], where $\langle\sigma_+(t+\tau)\sigma_-(t)\rangle$ can be calculated from the equations of single-time averages [Eqs. (4) and (5)] using the quantum regression theorem [1]

$$\frac{d}{d\tau}\begin{bmatrix} \langle\sigma_+(\tau)\sigma_-(0)\rangle \\ \langle\sigma_+(\tau)c_{\rm ccw}(0)\rangle \\ \langle\sigma_+(\tau)c_{\rm cw}(0)\rangle \end{bmatrix} = -i\mathbf{M}_c \begin{bmatrix} \langle\sigma_+(\tau)\sigma_-(0)\rangle \\ \langle\sigma_+(\tau)c_{\rm ccw}(0)\rangle \\ \langle\sigma_+(\tau)c_{\rm cw}(0)\rangle \end{bmatrix}. \tag{6}$$

The above equations can be solved via the Laplace transform with the initial conditions $\langle\sigma_+(0)\sigma_-(0)\rangle = 1$, $\langle\sigma_+(0)c_{\rm ccw}(0)\rangle = 0$, and $\langle\sigma_+(0)c_{\rm cw}(0)\rangle = 0$. The SE spectrum of the QE is expressed as (see Appendix B for a detailed derivation)

$$S(\omega) = \frac{1}{\pi}\frac{\Gamma(\omega)}{[\omega - \omega_c - \Delta(\omega)]^2 + \left[\frac{\Gamma(\omega)}{2}\right]^2}, \tag{7}$$

where $\Gamma(\omega) = -2g^2\,\mathrm{Im}[\chi(\omega)]$ is the local coupling strength and $\Delta(\omega) = g^2\,\mathrm{Re}[\chi(\omega)]$ denotes the photonic Lamb shift, with $\chi(\omega)$ being the response function of the CEP cavity:

$$\chi(\omega) = \frac{2}{(\omega-\omega_c) + i\frac{\kappa}{2}} - \frac{i\kappa e^{i\phi}}{\left[(\omega-\omega_c) + i\frac{\kappa}{2}\right]^2}. \tag{8}$$

The SE dynamics of the QE can be retrieved from $\mathcal{F}[S(\omega)]$, the Fourier transform of the SE spectrum.

Equations (1)–(8) constitute the basic theoretical framework for studying the cavity quantum electrodynamics in the CEP cavity. In the following sections, we derive the conditions of a single-photon DBS in the CEP cavity based on Eqs. (4) and (5).

B. VacancyLike dressed bound state

The coupled cavity is the simplest model that supports the vacancylike DBS, where the QE interacts with one of two cavities [26]. At first glance our model is different from the coupled cavity proposed in Ref. [26], but it would be the same if the basis of the cavity modes were changed. To find the condition of the vacancylike DBS in the CEP cavity, we rewrite $c_{\rm ccw}$ and $c_{\rm cw}$ in terms of the operators that represent the standing-wave modes c_1 and c_2 [37]:

$$c_{\rm cw} = \frac{1}{\sqrt{2}}(c_1 + c_2), \quad c_{\rm ccw} = \frac{1}{\sqrt{2}}(c_1 - c_2). \tag{9}$$

Substituting Eq. (9) into Eq. (5), we obtain $d\vec{s}/dt = -i\mathbf{M}_s\vec{s}$, with $\vec{s} = [\langle\sigma_-\rangle, \langle c_1\rangle, \langle c_2\rangle]^T$. The matrix $\mathbf{M}_s$ takes the form

$$\mathbf{M}_s = \begin{bmatrix} \omega_c & \sqrt{2}g & 0 \\ \sqrt{2}g & \omega_c - i\frac{\kappa(1+e^{i\phi})}{2} & i\frac{\kappa}{2}e^{i\phi} \\ 0 & -i\frac{\kappa}{2}e^{i\phi} & \omega_c - i\frac{\kappa(1-e^{i\phi})}{2}. \end{bmatrix} \tag{10}$$

Equation (10) shows that the QE is decoupled from the standing-wave mode c_2. The vacancylike DBS forms when the decay of c_2 is vanishing, i.e., $\phi = 2n\pi$ (n is an integer). In this case, the eigenstate is

$$|\psi_{VL}\rangle = \left(\frac{-i\kappa}{\sqrt{8g^2+\kappa^2}}, 0, \frac{2\sqrt{2}g}{\sqrt{8g^2+\kappa^2}}\right)^T, \tag{11}$$

with energy $\omega_{VL} = \omega_c$, the same as in the bare QE. Equation (11) indicates that the photon cannot be found at c_1 since its wave function is zero. As a consequence, the DBS can exist if we utilize the dissipative coupling of the cavity to a semi-infinite waveguide. Our model is thus different from the original model reported in the previous work [26] in terms of the method of coupling between two cavity modes, i.e., waveguide-mediated dissipative coupling instead of coherent coupling. Accordingly, the standing-wave mode c_1 is called the vacancy cavity. Figure 1(b) illustrates the concept of the vacancylike DBS in our model.

The existence of a vacancylike DBS can be confirmed by inspecting the spectral density of the CEP cavity, which is given by $J(\omega) = \mathrm{Re}\int_{-\infty}^{+\infty} d\tau e^{i\omega\tau} 2g^2\langle c_1^\dagger(\tau)c_1(0)\rangle$ for $\phi = 2n\pi$ [38,39], where the two-time correlation $\langle c_1^\dagger(\tau)c_1(0)\rangle$ can be calculated in a fashion similar to $\langle\sigma_+^\dagger(\tau)\sigma_-(0)\rangle$ using the quantum regression theorem. With the initial conditions $\langle c_1^\dagger(0)c_1(0)\rangle = 1$ and $\langle c_1^\dagger(0)c_2(0)\rangle = 0$, the spectral density can be analytically obtained:

$$J(\omega) = \frac{2g^2\kappa}{\pi}\left[\frac{\omega-\omega_c}{(\omega-\omega_c)^2 + \left(\frac{\kappa}{2}\right)^2}\right]^2. \tag{12}$$

Equation (12) indicates that on resonance ($\omega = \omega_c$) the spectral density is zero, implying a null electric-field amplitude at the location of the QE. Physically, this means that there is no available channel for the QE to decay, consistent with the nature of the vacancylike DBS. Figure 2 compares the analytical spectral density of a realistic CEP cavity (pink solid line) with the numerical results obtained from electromagnetic simulations (pink circles), where good agreement can be seen. The insets in Fig. 2 show the electric-field distribution at $J(\omega) = 0$, where we can see that the QE is located at a node of cavity modes and thus decoupled from c_1, contract to the conventional Lorentz cavity (blue line and circles), i.e., the CEP cavity without the mirror, where the QE locates exactly the antinode of the standing-wave mode. We thus understand that in a CEP cavity, the physical origin of a vacancylike DBS can be interpreted as being a result of the destructive

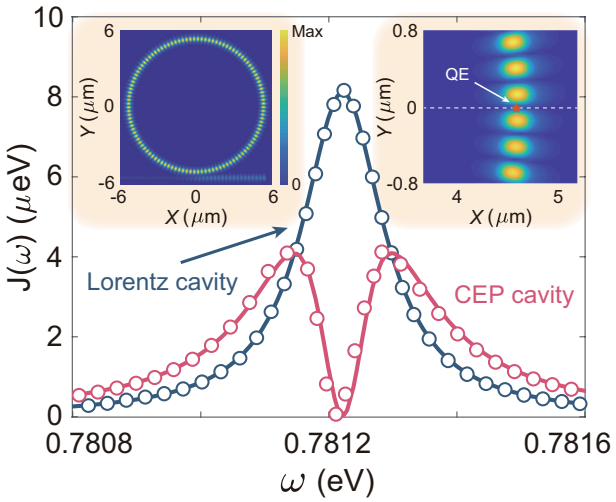

FIG. 2. Spectral density of a realistic CEP cavity with the following parameters: outer radius $R = 5\,\mu\text{m}$, width $w = 0.25\,\mu\text{m}$, refractive index $n_c = 3.47$, edge-to-edge separation to the waveguide $d = 0.2\,\mu\text{m}$. The width of the waveguide is d, and the mirror is made of 100-nm-thick silver. The refractive index of the background medium is $n_b = 1.44$. The blue circles plot the numerical results of the Lorentz cavity (CEP cavity without the mirror at the end), while the blue solid line shows the fitting results with the Lorentz spectral function. The pink solid line and circles represent the analytical and numerical results of the CEP cavity, respectively. The insets show the electric-field distribution of vacancylike DBS.

interference between the cavity field of the CCW mode and the reflected field of the CW mode.

Figure 3(a) shows that the SE spectrum is a triplet deviated from the DBS, with a Fano-type line shape around the cavity resonance. As the QE energy approaches the cavity resonance, the central peak in the SE spectrum becomes sharper and goes upwards; on resonance ($\omega_0 = \omega_c$) the central peak disappears, implying the formation of a vacancylike DBS. In this case, the SE spectrum exhibits a symmetrical Rabi splitting with a width of approximately $\sqrt{2}g$.

Figure 3(b) plots the time evolution of the population on the excited QE. It can be seen that the population of the QE can be fractionally trapped for various g/κ. As the eigenstate $|\psi_{VL}\rangle$ indicates, the steady-state population remains finite but decreases as g increases due to the stronger population transfer from the QE to the cavity. By contrast, the population of c_1 is depleted at the steady state (blue dashed line), as expected.

Since the vacancylike DBS occurs in the case of resonant QE-cavity coupling, it is beneficial for numerous quantum-optics applications, especially those involving energy transfer mediated by the cavity, such as the spontaneous entanglement generation (SEG) between qubits [4,40,41]. It is straightforward to extend our model to the multi-QE case by replacing H in Eq. (1) with the multi-QE Hamiltonian H^M, which is given by $H^M = H_0^M + H_I^M$, where $H_0^M = \omega_0 \sum_i \sigma_+^{(i)}\sigma_-^{(i)} + \omega_c c_{\text{ccw}}^\dagger c_{\text{ccw}} + \omega_c c_{\text{cw}}^\dagger c_{\text{cw}}$ and $H_I^M = \sum_i g_i(c_{\text{ccw}}^\dagger \sigma_-^{(i)} + \sigma_+^{(i)} c_{\text{ccw}}) + \sum_i g_i(c_{\text{cw}}^\dagger \sigma_-^{(i)} + \sigma_+^{(i)} c_{\text{cw}})$. With an initially excited qubit, the generated entanglement between two qubits is quantified by the concurrence $C(t) = 2|C_{eg}(t)C_{ge}^*(t)|$ [40,42], where $C_{eg}(t)$ and $C_{ge}(t)$ are the probability amplitudes of two single-excitation states in which one qubit is in the excited state while the other is in the ground state (a detailed derivation is given in Appendix C). The inset in Fig. 3(c) shows an illustration of SEG mediated by the CEP cavity, where long-distance entanglement can be generated between two qubits. The results of $g_2 = g_1 = g$ are shown in Fig. 3(c), which shows that higher and faster steady-state entanglement can be achieved as g increases and reaches a maximum of 0.5 with $g/\kappa = 1$. Since the Q factor of the WGM cavity is typically 10^5 at near infrared [20], the vacancylike DBS allows for fast and perfect entanglement without requiring a demanding coupling strength between the qubits and the cavity. In addition, we can see that Figs. 3(b) and 3(c) present opposite trends for large g. This indicates that the strong population transfer from the QE to cavity is unfavorable for population trapping of a single QE but can lead to an efficient QE-QE interaction mediated by the cavity and thus is beneficial for achieving SEG with long-lived entanglement.

We consider identical g for two QEs in Fig. 3(c); however, this is hard to realize in experiments due to the difficulty of precisely controlling the QEs' locations. We study the impact of nonidentical g on SEG in Fig. 6 in Appendix C. We see that

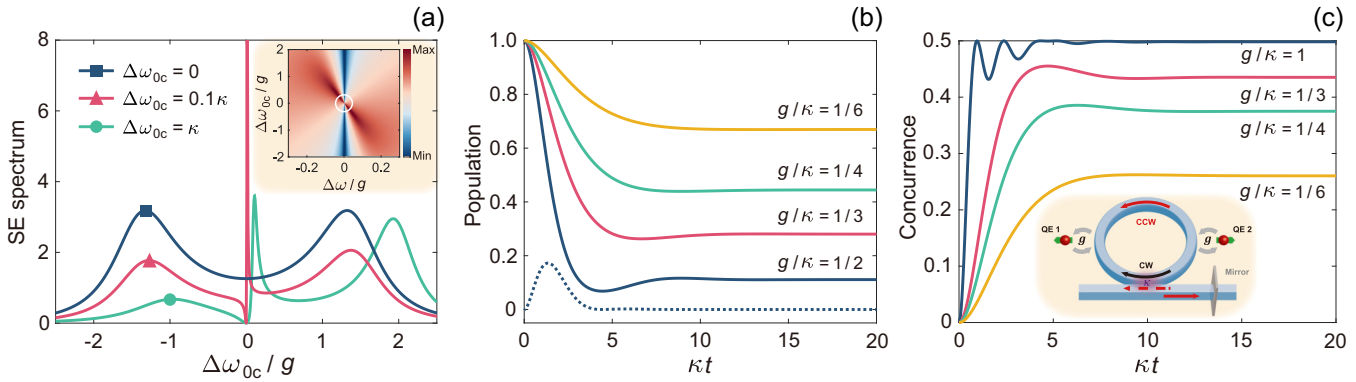

FIG. 3. (a) SE spectrum versus the QE-cavity detuning $\Delta\omega_{0c} = \omega_0 - \omega_c$ for $g = \kappa$. The white circle in the inset indicates the vacancylike DBS. (b) and (c) SE dynamics and dynamical concurrence of vacancylike DBS with an excited QE for various g/κ, respectively. The blue dashed line in (b) shows the population of c_1 for $g/\kappa = 1/2$. The inset in (c) illustrates the configuration of SEG.

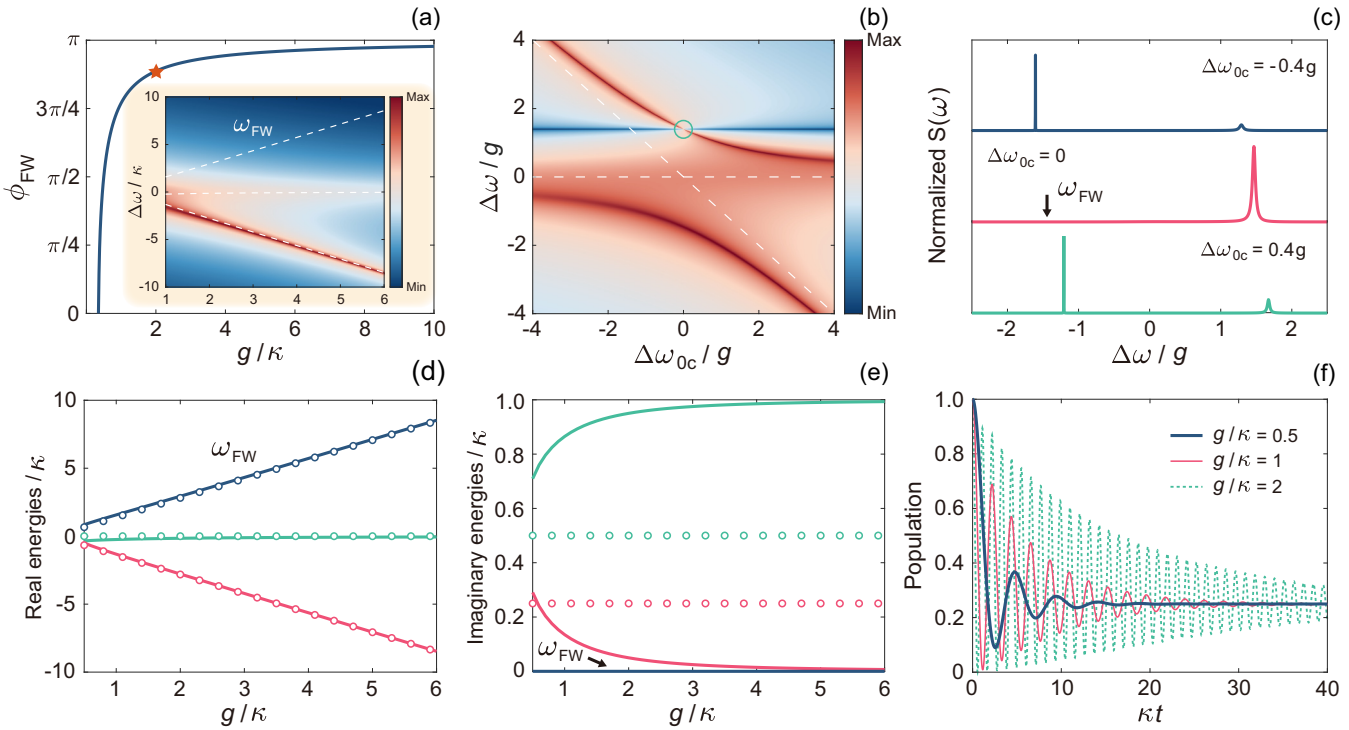

FIG. 4. (a) Condition of the Friedrich-Wintgen DBS versus g/κ. The red star indicates the parameters for (b). The inset shows the corresponding SE spectrum, where the white dashed lines track the real eigenenergies. (b) Logarithmic plot of the SE spectrum versus the QE-cavity detuning $\Delta\omega_{0c}$. (c) SE spectra for $\Delta\omega_{0c} = -0.4g$, 0, and $0.4g$. The black arrow indicates the energy of the vanishing Rabi peak. (d) and (e) The real and imaginary parts of eigenenergies versus g/κ, respectively, for the CEP cavity with the Friedrich-Wintgen DBS (solid lines) and Lorentz cavity (circles). Note that the blue circles are overlapped by the pink ones in (e). (f) SE dynamics with the Friedrich-Wintgen DBS for various g/κ.

the concurrence can be enhanced or reduced according to the values of g_2/g_1 and g/κ, but the entanglement of two QEs can still be achieved in the steady state. This result is attributed to the feature of the vacancylike DBS in which its condition is irrespective of g. The results thus show the vacancylike DBS is a promising candidate for robust SEG.

C. Friedrich-Wintgen dressed bound state

In addition to the vacancylike DBS, the CEP cavity supports another type of DBS that has a mechanism similar to the Friedrich-Wintgen bound states in the continuum (BICs) [29,43–45]. The right panel of Fig. 1(c) shows a schematic illustration of Friedrich-Wintgen BICs for coupled resonances, where the radiation of two cavities into the same waveguide gives rise to the via-the-continuum dissipative coupling. When the coherent coupling of two cavities J exists, the complete destructive interference of two cavities, i.e., the BIC, can be formed at some specific values of the continuous parameter. The cavity modes in the CEP cavity couple in a way similar to that of Friedrich-Wintgen BICs, as the left panel of Fig. 1(c) depicts, except the coherent coupling of two cavity modes is replaced by the indirect coupling through the QE and the waveguide-mediated coupling is unidirectional.

To derive the condition of the Friedrich-Wintgen DBS in the CEP cavity, we recast $\mathbf{M}_c$ in the following form [43]:

$$\mathbf{M}_c = H_B - i\Gamma, \tag{13}$$

with the Hermitian part giving rise to real energy for the DBS,

$$H_B = \begin{bmatrix} \omega_c & g & g \\ g & \omega_c & i\frac{\kappa}{2}e^{-i\phi} \\ g & -i\frac{\kappa}{2}e^{i\phi} & \omega_c \end{bmatrix}, \tag{14}$$

and the dissipative operator governing the imaginary part of the eigenenergies,

$$\Gamma = D^\dagger D = \begin{bmatrix} 0 & 0 & 0 \\ 0 & \frac{\kappa}{2} & \frac{\kappa}{2}e^{-i\phi} \\ 0 & \frac{\kappa}{2}e^{i\phi} & \frac{\kappa}{2} \end{bmatrix}. \tag{15}$$

Subsequently, we can determine the coupling matrix $D = (0, \sqrt{\kappa/2}, \sqrt{\kappa/2}e^{-i\phi})$ and introduce an un-normalized null vector of D, $|\psi_0\rangle = (\alpha, -e^{-i\phi}, 1)^T$, satisfying $D|\psi_0\rangle = 0$, where α is an undetermined coefficient. The Friedrich-Wintgen DBS appears when $|\psi_0\rangle$ fulfills $H_B|\psi_0\rangle = \omega_{FW}|\psi_0\rangle$. The solutions yield the energy and condition of the Friedrich-Wintgen DBS,

$$\omega_{FW} = \omega_c \pm \frac{\sqrt{8g^2 - \kappa^2}}{2}, \tag{16}$$

$$\phi_{FW} = -i \ln\left(-\frac{(4g^2 - \kappa^2) \pm i\kappa\sqrt{8g^2 - \kappa^2}}{4g^2}\right). \tag{17}$$

Figure 4(a) plots ϕ_{FW} versus g/κ, showing that ϕ_{FW} tends to π for a large g. With ϕ_{FW}, there are only two peaks seen in the SE spectrum; the Rabi peak corresponding to

the Friedrich-Wintgen DBS is invisible due to the vanishing linewidth, as the inset of Fig. 4(a) shows. On the other hand, by continuously varying the QE-cavity detuning, we observe an unusual behavior of strong-coupling anticrossing in Figs. 4(b) and 4(c), where the linewidth of one of the bands is narrower and the peak disappears at a specific frequency [on resonance here; see the green circle in Fig. 4(b) and the pink line in Fig. 4(c)], a signature of Friedrich-Wintgen-type bound states [27,46]. The real and imaginary parts of the eigenenergies versus g/κ are plotted in Figs. 4(d) and 4(e), respectively, which show that the real energies of the CEP cavity are nearly the same as those of the Lorentz cavity, while the imaginary parts are dissimilar. It is worth noting that the linewidth of the remaining Rabi peak significantly narrows for $g > \kappa$ compared to that of the Lorentz cavity and approaches zero as g gradually increases [see the thin solid line in Fig. 4(e)]. The corresponding linewidth is found to be $\sim[1+\cos(\phi_{\rm FW})]/2$ for $g \gg \kappa$. The linewidth narrowing of dressed states is accompanied by the decay suppression of Rabi oscillation in the time domain [see the SE dynamics for various g/κ in Fig. 4(f)]. Therefore, for the Friedrich-Wintgen DBS, a large g benefits achieving a long decoherence time.

Although both are DBSs in the same cavity QED system, there are two great differences between the vacancylike DBS and the Friedrich-Wintgen DBS. One difference is that the steady-state population of the former depends on the coupling strength g [see Fig. 3(b)], while the latter does not, as Fig. 4(f) shows. We find that half the energy can be trapped in the system via the Friedrich-Wintgen DBS and the steady-state population of the QE is 1/4 irrespective of g. Another difference lies in the energy of the DBS. The energy of the vacancylike DBS is equal to the bare QE for any g, while the Friedrich-Wintgen DBS occurs at one of the anharmonic energy levels in which the energy spacing is proportional to g. This feature offers the Friedrich-Wintgen DBS a unique potential for single-photon generation utilizing the photon-blockade effect [5,47,48]. Figure 5 compares the performance of single-photon blockade of the CEP cavity with that of the Lorentz cavity. It shows that the best performance is achieved at the Friedrich-Wintgen DBS (vertical dashed line), where both the single-photon efficiency $I_c = \langle c_{\rm cw}^\dagger c_{\rm cw}\rangle$ and the photon correlation $g^{(2)}(0) = \langle c_{\rm cw}^\dagger c_{\rm cw}^\dagger c_{\rm cw} c_{\rm cw}\rangle / I_c^2$ manifest a remarkable enhancement of more than two orders of magnitude compared to the dressed states in the conventional Lorentz cavity (dashed lines).

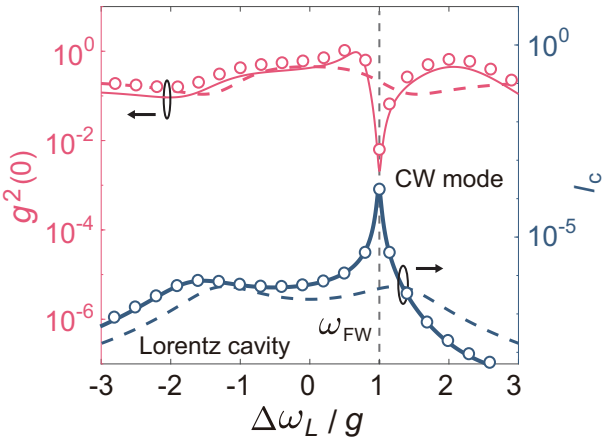

FIG. 5. Comparison of the single-photon blockade of the CEP cavity (circles for numerical results and solid lines for analytical results) with the Lorentz cavity (dashed lines). The results are obtained by implementing a driving Hamiltonian $H_d = \Omega(e^{-i\omega_L t}\sigma_+ + e^{i\omega_L t}\sigma_-)$ and a Liouvillian superoperator $\gamma\mathcal{L}[\sigma_-]\rho$ for QE dissipation in Eq. (1). The numerical results are obtained using QUTIP [49]. The parameters used in the simulations are $g = \kappa/2$, $\gamma = \kappa/20$, and $\Omega = 10^{-2}\gamma$. The analytical expressions of I_c and $g^{(2)}(0)$ are derived in Appendix D. The vertical dashed line indicates ω_{FW} given by Eq. (16).

III. CONCLUSION

In conclusion, we demonstrated and unveiled the origin of dressed bound states (DBSs) in a prototypical microring resonator operating at chiral exceptional points (CEPs), which are classified into two types, the vacancylike and Friedrich-Wintgen-type bound states. DBSs studied in this work exist in the single-photon manifold, while the principles can be applied to higher-excitation manifolds for exploring multiphoton DBSs. Besides the spontaneous entanglement generation and single-photon generation demonstrated here, we envision prominent advantages of DBSs in diverse applications, such as quantum logic gate operation and quantum sensing, due to the long decoherence time and extremely sharp line shape of DBSs. We believe our work not only deepens the understanding of DBSs at CEPs but also paves the way for harnessing the non-Hermitian physics to manipulate quantum states.

ACKNOWLEDGMENTS

Y.L. acknowledges the support of the National Natural Science Foundation of China (Grants No. 62205061 and No. 12274192). Z.L. is supported by the National Key R&D Program of China (Grant No. 2021YFA1400800) and the Natural Science Foundations of Guangdong (Grant No. 2021A1515010039).

APPENDIX A: DERIVATION OF THE EXTENDED CASCADED QUANTUM MASTER EQUATION

The extended cascaded quantum master equation (QME) in Eq. (1) can be derived by tracing out the waveguide modes based on the model depicted in Fig. 1(c). The system Hamiltonian including the waveguide modes is written as ($\hbar = 1$)

$$H_S = H + H_B + H_{SB}, \tag{A1}$$

where $H = H_0 + H_I$ is given in Eq. (1). H_B is the free Hamiltonian of the waveguide,

$$H_B = \int d\omega \omega b_R^\dagger b_R, \tag{A2}$$

and H_{SB} describes the Hamiltonian of the cavity-waveguide interaction,

$$H_{SB} = i \sum_{j=ccw,cw} \int d\omega \sqrt{\frac{\kappa}{2\pi}} b_R^\dagger e^{-ikx_j} c_j + \text{H.c.}, \tag{A3}$$

where b_R is the bosonic annihilation operator of the right-propagating waveguide mode with frequency ω and wave vector $k = \omega_c/v$, with v being the group velocity. x_{ccw} and x_{cw} are the locations of the CCW mode and the mirrored CW mode, respectively. Applying the transformation $\widetilde{H} = UHU^\dagger - idU/dtU^\dagger$ with $U = \exp[i(\omega_c \sum_{j=\text{ccw,cw}} c_j^\dagger c_j + \int d\omega \omega b_R^\dagger b_R)]$, we have

$$\widetilde{H}_{SB}(t) = i \sum_{j=\text{ccw,cw}} \int d\omega \sqrt{\frac{\kappa}{2\pi}} b_R^\dagger e^{i(\omega-\omega_c)t} e^{-i\omega x_j/v} c_j + \text{H.c.} \tag{A4}$$

The equation of motion of b_R can be obtained from the Heisenberg equation,

$$\frac{d}{dt} b_R(t) = \sum_{j=\text{ccw,cw}} \sqrt{\frac{\kappa}{2\pi}} c_j e^{i(\omega-\omega_c)t} e^{-i\omega x_j/v}. \tag{A5}$$

The above equation can be formally integrated to obtain

$$b_R(t) = \sum_{j=\text{ccw,cw}} \int_0^t d\tau \sqrt{\frac{\kappa}{2\pi}} c_j e^{i(\omega-\omega_c)\tau} e^{-i\omega x_j/v}, \tag{A6}$$

where we have taken $b_R(0) = 0$ since the waveguide is initially in the vacuum state. On the other hand, the equation of motion of the arbitrary operator O is given by

$$\frac{d}{dt} O(t) = \sum_{j=\text{ccw,cw}} \int d\omega \sqrt{\frac{\kappa}{2\pi}} \{b_R^\dagger(t) e^{i(\omega-\omega_c)t} e^{-i\omega x_j/v} [O(t), c_j(t)] - [O(t), c_j^\dagger(t)] b_R(t) e^{-i(\omega-\omega_c)t} e^{i\omega x_j/v}\}. \tag{A7}$$

Substituting $b_R(t)$ into the above equation, we have

$$\frac{d}{dt} O(t) = \frac{\kappa}{2\pi} \sum_{j,l=\text{ccw,cw}} \int_0^t d\tau \int d\omega \left\{e^{i(\omega-\omega_c)(t-\tau)} e^{-i\omega x_j/v} c_l^\dagger(\tau) [O(t), c_j(t)] - [O(t), c_j^\dagger(t)] c_l(\tau) e^{-i(\omega-\omega_c)(t-\tau)} e^{i\omega x_{jl}/v}\right\}, \tag{A8}$$

where $x_{jl} = x_j - x_l$. We apply the Markov approximation by assuming the time delay x_{jl}/v between the CCW mode and the mirrored CW mode can be neglected. Therefore,

$$\begin{aligned} \frac{\kappa}{2\pi} \sum_{l=\text{ccw,cw}} \int_0^t d\tau \int d\omega e^{i(\omega-\omega_c)(t-\tau)} e^{-i\omega x_{jl}/v} c_l^\dagger(\tau) &= \kappa \sum_{l=\text{ccw,cw}} \int_0^t d\tau \delta\left(t - \frac{x_{jl}}{v} - \tau\right) e^{-ikx_{jl}} c_l^\dagger(\tau) \\ &\approx \frac{\kappa}{2} c_j^\dagger(t) + \kappa \sum_{l=\text{ccw,cw}} \Theta\left(t - \frac{x_{jl}}{v}\right) e^{-ikx_{jl}} c_l^\dagger(t), \end{aligned} \tag{A9}$$

where $x_{jl} > 0$ and $\Theta(t)$ is the step function. With Eq. (A9) and taking the averages of Eq. (A8), we have

$$\begin{aligned} \frac{d}{dt} \langle O(t) \rangle = &\frac{\kappa}{2} \sum_{j=\text{ccw,cw}} \{\langle c_j^\dagger(t) [O(t), c_j(t)] \rangle - \langle [O(t), c_j^\dagger(t)] c_j(t) \rangle\} \\ &+ \kappa \sum_{j,l=\text{ccw,cw}, j\neq l} \{e^{-ikx_{jl}} \langle c_l^\dagger(t) [O(t), c_j(t)] \rangle - e^{ikx_{jl}} \langle [O(t), c_j^\dagger(t)] c_l(t) \rangle\}. \end{aligned} \tag{A10}$$

Since $\langle O(t) \rangle = \text{Tr}[O(t)\rho(0)] = \text{Tr}[O\rho(t)]$, we can simplify the averages of operators in the above equation by using the cyclic property of the trace. For example,

$$\langle [O(t), c_j^\dagger(t)] c_j(t) \rangle = \text{Tr}[Oc_j^\dagger c_j \rho(t) - c_j^\dagger O c_j \rho(t)] = \text{Tr}[Oc_j^\dagger c_j \rho(t) - Oc_j \rho(t) c_j^\dagger] = \text{Tr}\{O[c_j^\dagger, c_j \rho(t)]\}. \tag{A11}$$

Therefore, we can obtain a QME in the following form:

$$\frac{d}{dt} \rho(t) = -i[H, \rho(t)] + \frac{\kappa}{2} \sum_{j=\text{ccw,cw}} \{[c_j, \rho(t) c_j^\dagger] - [c_j^\dagger, c_j \rho(t)]\} + \kappa \sum_{j,l=\text{ccw,cw}, j\neq l} \{e^{-ikx_{jl}} [c_j, \rho(t) c_l^\dagger] - e^{ikx_{jl}} [c_j^\dagger, c_l \rho(t)]\}. \tag{A12}$$

Note that $kx_{jl} = \phi$, and thus, $j = \text{cw}$ and $l = \text{ccw}$ in the third term on the right-hand side. In addition, the second term on the right-hand side can be expanded and rewritten using the Liouvillian superoperator. We thus arrive at the extended cascaded QME in Eq. (1).

APPENDIX B: DERIVATION OF THE SPONTANEOUS EMISSION SPECTRUM

The spontaneous emission (SE) spectrum, also called the polarization spectrum, reflects the local dynamics of a

quantum emitter (QE). The SE spectrum is given by $S(\omega) = \lim_{t\to\infty} 2\,\mathrm{Re}[\int_0^\infty d\tau\,\langle\sigma_+(t+\tau)\sigma_-(t)\rangle e^{i\omega\tau}]$, where the correlation $\langle\sigma_+(t+\tau)\sigma_-(t)\rangle$ can be solved from Eqs. (4) and (5) using the quantum regression theorem, which yields the following equations of motion:

$$\frac{d}{d\tau}\begin{bmatrix}\langle\sigma_+(\tau)\sigma_-(0)\rangle\\ \langle\sigma_+(\tau)c_{\mathrm{ccw}}(0)\rangle\\ \langle\sigma_+(\tau)c_{\mathrm{cw}}(0)\rangle\end{bmatrix} = \begin{bmatrix}\omega_0 & g & g\\ g & \omega_c - i\frac{\kappa}{2} & 0\\ g & -i\kappa e^{i\phi} & \omega_c - i\frac{\kappa}{2}\end{bmatrix} \times \begin{bmatrix}\langle\sigma_+(\tau)\sigma_-(0)\rangle\\ \langle\sigma_+(\tau)c_{\mathrm{ccw}}(0)\rangle\\ \langle\sigma_+(\tau)c_{\mathrm{cw}}(0)\rangle\end{bmatrix}. \tag{B1}$$

Using the initial conditions $\langle\sigma_+(0)\sigma_-(0)\rangle = 1$, $\langle\sigma_+(0)c_{\mathrm{ccw}}(0)\rangle = 0$, and $\langle\sigma_+(0)c_{\mathrm{cw}}(0)\rangle = 0$, the above correlations can be easily obtained by taking the Laplace transform $\langle O(\tau)\rangle \to \langle O(s)\rangle$,

$$s\begin{bmatrix}\langle\sigma_+\sigma_-(s)\rangle\\ \langle\sigma_+c_{\mathrm{ccw}}(s)\rangle\\ \langle\sigma_+c_{\mathrm{cw}}(s)\rangle\end{bmatrix} = \begin{bmatrix}\omega_0 & g & g\\ g & \omega_c - i\frac{\kappa}{2} & 0\\ g & -i\kappa e^{i\phi} & \omega_c - i\frac{\kappa}{2}\end{bmatrix} \times \begin{bmatrix}\langle\sigma_+\sigma_-(s)\rangle\\ \langle\sigma_+c_{\mathrm{ccw}}(s)\rangle\\ \langle\sigma_+c_{\mathrm{cw}}(s)\rangle\end{bmatrix} + \begin{bmatrix}1\\0\\0\end{bmatrix}. \tag{B2}$$

The solutions are given by

$$\langle\sigma_+\sigma_-(s)\rangle = \frac{1}{s + i\omega_0 + \frac{g^2}{s+i(\omega_c - i\frac{\kappa}{2})}\left[2 - \frac{\kappa e^{i\phi}}{s+i(\omega_c - i\frac{\kappa}{2})}\right]}. \tag{B3}$$

Transforming into the frequency domain [Eq. (B3)] by replacing $s = -i\omega$, we have

$$\left(-i(\omega-\omega_0) + \frac{2g^2}{-i(\omega-\omega_c) + \kappa + i\frac{\left(\frac{\kappa}{2}\right)^2}{\omega-\omega_c}}\right)\langle\sigma_+\sigma_-(\omega)\rangle = 1. \tag{B4}$$

Therefore,

$$\langle\sigma_+\sigma_-(\omega)\rangle = \frac{i}{(\omega-\omega_0) - g^2\left\{\frac{2}{(\omega-\omega_c)+i\frac{\kappa}{2}} - \frac{i\kappa e^{i\phi}}{\left[(\omega-\omega_c)+i\frac{\kappa}{2}\right]^2}\right\}}. \tag{B5}$$

We identify the response function of the CEP cavity as

$$\chi(\omega) = \frac{2}{(\omega-\omega_c)+i\frac{\kappa}{2}} - \frac{i\kappa e^{i\phi}}{\left[(\omega-\omega_c)+i\frac{\kappa}{2}\right]^2}, \tag{B6}$$

where the first term on the right-hand side denotes the usual Lorentz response, with the factor of 2 representing the coupling of the QE to two cavity modes. The second term on the right-hand side demonstrates the characteristic of squared Lorentz response and thus is contributed by the CEP. Equation (B5) can be rewritten as

$$\langle\sigma_+\sigma_-(\omega)\rangle = \frac{i}{\omega - \omega_0 - \Delta(\omega) + i\frac{\Gamma(\omega)}{2}}. \tag{B7}$$

Therefore, the SE spectrum is expressed as

$$S(\omega) = \frac{2}{\pi}\,\mathrm{Re}[\langle\sigma_+\sigma_-(\omega)\rangle] = \frac{1}{\pi}\frac{\Gamma(\omega)}{[\omega-\omega_0-\Delta(\omega)]^2 + \left[\frac{\Gamma(\omega)}{2}\right]^2}, \tag{B8}$$

with the photon-induced Lamb shift

$$\Delta(\omega) = g^2\,\mathrm{Re}[\chi(\omega)] = \frac{\left[(\omega-\omega_c)^2 - \left(\frac{\kappa}{2}\right)^2\right][2(\omega-\omega_c) + \kappa\sin(\phi)] + \kappa^2(\omega-\omega_c)[1-\cos(\phi)]}{\left[(\omega-\omega_c)^2 + \left(\frac{\kappa}{2}\right)^2\right]^2} \tag{B9}$$

and the local coupling strength

$$\Gamma(\omega) = -2g^2\,\mathrm{Im}[\chi(\omega)] = -2\frac{\left[(\omega-\omega_c)^2 - \left(\frac{\kappa}{2}\right)^2\right]\kappa[1-\cos(\phi)] - \kappa(\omega-\omega_c)[2(\omega-\omega_c) + \kappa\sin(\phi)]}{\left[(\omega-\omega_c)^2 + \left(\frac{\kappa}{2}\right)^2\right]^2}. \tag{B10}$$

For the vacancylike DBS ($\phi = 2n\pi$), the local coupling strength is

$$\Gamma(\omega) = 4g^2\kappa\left[\frac{\omega-\omega_c}{(\omega-\omega_c)^2 + \left(\frac{\kappa}{2}\right)^2}\right]^2 = 2\pi J(\omega), \tag{B11}$$

where $J(\omega)$ is given in Eq. (12).

APPENDIX C: SPONTANEOUS ENTANGLEMENT GENERATION AT THE VACANCYLIKE BOUND STATE

The system Hamiltonian for spontaneous entanglement generation (SEG) is written as

$$H^M = H_0^M + H_I^M, \tag{C1}$$

where H_0^M and H_I^M are given by

$$H_0^M = \omega_c \sum_{j=1,2} \sigma_+^{(j)}\sigma_-^{(j)} + \omega_c c_{\rm ccw}^\dagger c_{\rm ccw} + \omega_c c_{\rm cw}^\dagger c_{\rm cw}, \tag{C2}$$

$$H_I^M = \sum_{j=1,2} g_i\big(\sigma_-^{(j)} c_{\rm ccw}^\dagger + c_{\rm ccw}\sigma_+^{(j)}\big) + g_i\big(\sigma_-^{(j)} c_{\rm cw}^\dagger + c_{\rm cw}\sigma_+^{(j)}\big). \tag{C3}$$

With the extended cascaded QME [Eq. (1)], we can obtain the effective Hamiltonian in the single-excitation subspace,

$$H_{\rm eff} = \omega_c \sum_{j=1,2} \sigma_+^{(j)}\sigma_-^{(j)} + \Big(\omega_c - i\frac{\kappa}{2}\Big)c_{\rm ccw}^\dagger c_{\rm ccw} + \Big(\omega_c - i\frac{\kappa}{2}\Big)c_{\rm cw}^\dagger c_{\rm cw} + \sum_{j=1,2} g_i\big(\sigma_-^{(j)} c_{\rm ccw}^\dagger + c_{\rm ccw}\sigma_+^{(j)}\big)$$
$$+ g_i\big(\sigma_-^{(j)} c_{\rm cw}^\dagger + c_{\rm cw}\sigma_+^{(j)}\big) - i\kappa e^{i\phi} c_{\rm ccw} c_{\rm cw}^\dagger. \tag{C4}$$

The corresponding state vector is given by

$$|\Psi(t)\rangle = C_{gg}(t)|gg00\rangle + C_{eg}(t)|eg00\rangle + C_{ge}(t)|ge00\rangle + C_{10}(t)|gg10\rangle + C_{01}(t)|gg01\rangle, \tag{C5}$$

where $|n_1 n_2 m p\rangle = |n_1\rangle \otimes |n_2\rangle \otimes |m\rangle \otimes |p\rangle$, with $|n_1\rangle$ and $|n_2\rangle$ representing that the QE is either in the excited state ($|n_1\rangle$, $|n_2\rangle = |e\rangle$) or in the ground state ($|n_1\rangle$, $|n_2\rangle = |g\rangle$) and $|m\rangle$ and $|p\rangle$ denoting that there are m photons in the CCW mode and p photons in the mirrored CW mode, respectively. With the Schrödinger equation $id|\Psi(t)\rangle/dt = H_{\rm eff}|\Psi(t)\rangle$, we can obtain the equations of coefficients:

$$i\frac{d}{dt}C_{eg}(t) = \omega_c C_{eg}(t) + g_1 C_{10}(t) + g_1 C_{01}(t), \tag{C6}$$

$$i\frac{d}{dt}C_{ge}(t) = \omega_c C_{ge}(t) + g_2 C_{10}(t) + g_2 C_{01}(t), \tag{C7}$$

$$i\frac{d}{dt}C_{10}(t) = \Big(\omega_c - i\frac{\kappa}{2}\Big)C_{10}(t) + g_1 C_{eg}(t) + g_2 C_{ge}(t), \tag{C8}$$

$$i\frac{d}{dt}C_{01}(t) = \Big(\omega_c - i\frac{\kappa}{2}\Big)C_{01}(t) + g_1 C_{eg}(t) + g_2 C_{ge}(t) - i\kappa e^{i\phi} C_{10}(t). \tag{C9}$$

For vacancylike DBS ($\phi = 2n\pi$), the above equations can be easily solved through the Laplace transform,

$$C_{eg}(t) = \frac{e^{(i\sqrt{2}g_s - \frac{\kappa}{2})t} g_1^2\big(4g_s^2 - i\sqrt{2}g_s\kappa\big) + e^{-(i\sqrt{2}g_s + \frac{\kappa}{2})t} g_1^2\big(4g_s^2 + i\sqrt{2}g_s\kappa\big) + g_s^2\big(8g_2^2 + \kappa^2\big)}{g_s^2(8g_s^2 + \kappa^2)}, \tag{C10}$$

$$C_{ge}(t) = \frac{e^{-(i\sqrt{2}g_s + \frac{\kappa}{2})t} g_1 g_2\big[4g_s^2\big(1 + e^{i2\sqrt{2}g_s t} - 2e^{(i\sqrt{2}g_s + \frac{\kappa}{2})t}\big) - i\sqrt{2}g_s\kappa(-1 + e^{i2\sqrt{2}g_s t})\big]}{g_s^2\big(8g_s^2 + \kappa^2\big)}, \tag{C11}$$

where $g_s = \sqrt{g_1^2 + g_2^2}$. Then the dynamical concurrence can be obtained as $C(t) = 2|C_{eg}(t)C_{ge}^*(t)|$.

In the main text, we consider the SEG of identical g. In Figs. 6(a) and 6(b), we investigate the concurrence versus g_2/g_1 for $g_1 = \kappa$ and $g_1 = \kappa/4$, respectively, where we can see that the identical g correspond to the highest concurrence for $g_1 = \kappa/4$, while $g_2 < g_1$ is beneficial for achieving higher concurrence for $g_1 = \kappa$. Steady-state concurrence as a function of g_1/κ and g_2/g_1 is shown in Fig. 6(c), which

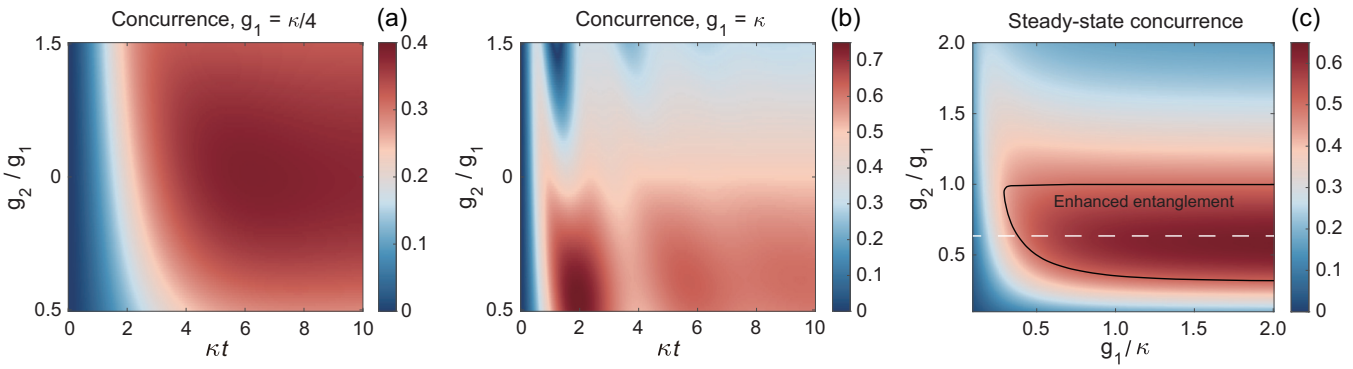

FIG. 6. (a) and (b) Dynamical concurrence versus g_2/g_1 for $g_1 = \kappa/4$ and $g_1 = \kappa$, respectively. (c) Steady-state concurrence as a function of g_1/κ and g_2/g_1. The white dashed line indicates the optimal g_2/g_1 for the maximum steady-state concurrence when $g_1/\kappa > 1$. The black solid line labels the parameter range of enhanced entanglement compared to the case of $g_2 = g_1$.

clearly shows that nonidentical g are beneficial to enhancing the entanglement of QEs with $g_1/\kappa > 0.5$ and g_2/g_1 in the range of $0.4 < g_2/g_1 < 1$.

APPENDIX D: SINGLE-PHOTON GENERATION AT THE FRIEDRICH-WINTGEN BOUND STATE

The single-photon generation through photon blockade requires weak coherent pumping. In this Appendix, we present a derivation of the analytical expressions for the average photon number and zero-time-delay second-order correlation function of the CW mode using perturbation theory. A driving Hamiltonian is implemented in the extended cascaded QME for the QE-driven case, which is

$$H_{\text{driving}} = \Omega(e^{-i\omega_L t}\sigma_+ + \sigma_- e^{i\omega_L t}), \tag{D1}$$

where ω_L is the frequency of the laser field and Ω is the driving strength. Applying the unitary transformation $U = \exp[-i\omega_L(c_{\text{ccw}}^\dagger c_{\text{ccw}} + c_{\text{cw}}^\dagger c_{\text{cw}} + \sigma_+\sigma_-)t]$, we can obtain the effective Hamiltonian

$$H_{\text{eff}}^t = H^t + EV, \tag{D2}$$

with

$$\begin{aligned} H^t = {} & \Delta_0\sigma_+\sigma_- + \Delta_c c_{\text{ccw}}^\dagger c_{\text{ccw}} + \Delta_c c_{\text{cw}}^\dagger c_{\text{cw}} \\ & + g(\sigma_- c_{\text{ccw}}^\dagger + c_{\text{ccw}}\sigma_+) + g(\sigma_- c_{\text{cw}}^\dagger + c_{\text{cw}}\sigma_+) \\ & - i\kappa e^{i\phi} c_{\text{ccw}} c_{\text{cw}}^\dagger \end{aligned} \tag{D3}$$

and

$$V = \Omega(\sigma_+ + \sigma_-), \tag{D4}$$

where $\Delta_0 = \Delta_{cL} - i\gamma/2$ and $\Delta_c = \Delta_{cL} - i\kappa/2$, with $\Delta_{cL} = \omega_c - \omega_L$ being the frequency detuning between the system and the laser field. E is a perturbative parameter of laser intensity. Since the evaluation of $g^{(2)}(0) = \langle c_{\text{cw}}^\dagger c_{\text{cw}}^\dagger c_{\text{cw}} c_{\text{cw}}\rangle / I_c^2$ requires calculating the second-order correlation function of the cavity operator, we expand the time-dependent wave function $|\Psi(t)\rangle$ in terms of E as $|\Psi(t)\rangle = \sum_{l=2} E^l |\psi_l(t)\rangle$, where we have truncated the state space by the two-excitation manifold, and as a result, $|\psi_l(t)\rangle$ is expressed as

$$|\psi_l(t)\rangle = \sum_{n+m+p\leqslant 2, n=0,1} C_{nmp}^l |n\rangle_e |m\rangle_{\text{ccw}} |p\rangle_{\text{cw}}, \tag{D5}$$

where C_{nmp}^l is the coefficient of quantum state $|n\rangle_e|m\rangle_{\text{ccw}}|p\rangle_{\text{cw}}$ in the l-order expansion, where there are m photons in the CCW mode and p photons in the CW mode, while the QE is either excited ($n = 1$) or unexcited ($n = 0$). For $l = 1$ and 2, the state vectors are given by

$$|\psi_1(t)\rangle = C_{100}^1|100\rangle + C_{010}^1|010\rangle + C_{001}^1|001\rangle, \tag{D6}$$

$$\begin{aligned} |\psi_2(t)\rangle = {} & C_{011}^2|011\rangle + C_{10}^2|110\rangle + C_{101}^2|101\rangle + C_{020}^2|020\rangle \\ & + C_{002}^2|002\rangle. \end{aligned} \tag{D7}$$

From the Schrödinger equation $id|\Psi(t)\rangle/dt = H_{\text{eff}}^t|\Psi(t)\rangle$, we have

$$i\frac{d}{dt}|\psi_0(t)\rangle = H^t|\psi_0(t)\rangle, \tag{D8}$$

$$i\frac{d}{dt}|\psi_l(t)\rangle = H^t|\psi_l(t)\rangle + V|\psi_{l-1}(t)\rangle. \tag{D9}$$

Substituting H^t [Eq. (D2)] and V [Eq. (D3)] into Eqs. (D8) and (D9), we can obtain the following equations of motion for coefficients:

$$i\frac{d}{dt}C_{100}^1 = \Delta_0 C_{100}^1 + gC_{010}^1 + gC_{001}^1 + \Omega, \tag{D10}$$

$$i\frac{d}{dt}C_{010}^1 = \Delta_c C_{010}^1 + gC_{100}^1, \tag{D11}$$

$$i\frac{d}{dt}C_{001}^1 = \Delta_c C_{001}^1 + gC_{100}^1 - i\kappa e^{i\phi} C_{010}^1, \tag{D12}$$

and $C_{000}^0 \approx 1$ due to the assumption of weak pumping. The above equations yield

$$C_{001}^1 = \Omega g \frac{\Delta_c + i\kappa e^{i\phi}}{D_1}, \tag{D13}$$

with

$$D_1 = \begin{vmatrix} \Delta_0 & g & g \\ g & \Delta_c & 0 \\ g & -i\kappa e^{i\phi} & \Delta_c \end{vmatrix}. \tag{D14}$$

Therefore, the average photon number of the CW mode is given by

$$I_c = \langle\Psi(0)|c_{\text{cw}}^\dagger c_{\text{cw}}|\Psi(0)\rangle \approx \left|C_{001}^1\right|^2 = \left|\Omega g \frac{\Delta_c + i\kappa e^{i\phi}}{D_1}\right|^2. \tag{D15}$$

We can see that the eigenvalues of D_1 are the same as the matrix $\mathbf{M}_c$ in Eq. (13), and thus, the cavity photon I_c diverges at the Friedrich-Wintgen DBS due to the zero decay (linewidth), and perfect single-photon purity can be achieved since $g^{(2)}(0) \propto I_c^{-2}$. This unphysical result comes from the truncation of state space with at most one excitation. I_c will remain finite when taking into account higher-order manifolds. However, the analytical expression of I_c predicts that the formation of a bound state in the single-excitation subspace can produce a prominent enhancement of both the efficiency and purity of single-photon blockade.

From Eq. (D9), we can also obtain the equations of a two-excitation subspace:

$$i\frac{d}{dt}C_{011}^2 = 2\Delta_c C_{011}^2 + gC_{101}^2 + gC_{110}^2 - i\sqrt{2}\kappa e^{i\phi} C_{020}^2, \tag{D16}$$

$$i\frac{d}{dt}C_{110}^2 = (\Delta_0 + \Delta_c)C_{110}^2 + \sqrt{2}gC_{020}^2 + gC_{011}^2 + \Omega C_{010}^1, \tag{D17}$$

$$\begin{aligned} i\frac{d}{dt}C_{101}^2 = {} & (\Delta_0 + \Delta_c)C_{101}^2 + gC_{011}^2 + \sqrt{2}gC_{002}^2 - ike^{i\phi}C_{110}^2 \\ & + \Omega C_{001}^1, \end{aligned} \tag{D18}$$

$$i\frac{d}{dt}C_{020}^2 = 2\Delta_c C_{020}^2 + \sqrt{2}gC_{110}^2, \tag{D19}$$

$$i\frac{d}{dt}C_{002}^2 = 2\Delta_c C_{002}^2 + \sqrt{2}gC_{101}^2 - i\sqrt{2}\kappa e^{i\phi} C_{011}^2. \tag{D20}$$

We thus can obtain

$$C_{002}^{2} = 2\sqrt{2}gD_{2}^{-1}\big(C_{001}^{1}\{\Delta_c[2\Delta_c(\Delta_c+\Delta_0)-3g^2]+i\kappa e^{i\phi}[\Delta_c(\Delta_c+\Delta_0)-2g^2]\} + C_{010}^{1}\{\Delta_c g^2+i\kappa e^{i\phi}[\Delta_c(3\Delta_c+\Delta_0)+g^2]-\kappa^2 e^{2i\phi}(2\Delta_c+\Delta_0)\}\big), \tag{D21}$$

with

$$D_2 = \begin{vmatrix} 2\Delta_c & g & g & -i\sqrt{2}\kappa e^{i\phi} & 0 \\ g & \Delta_0+\Delta_c & 0 & \sqrt{2}g & 0 \\ g & -i\kappa e^{i\phi} & \Delta_0+\Delta_c & 0 & \sqrt{2}g \\ 0 & \sqrt{2}g & 0 & 2\Delta_c & 0 \\ -i\sqrt{2}\kappa e^{i\phi} & 0 & \sqrt{2}g & 0 & 2\Delta_c \end{vmatrix} = 4D_1[-2g^2+\Delta_c(3\Delta_c+2\Delta_0)]+4\Delta_c^4(2\Delta_c+\Delta_0). \tag{D22}$$

Then the zero-time-delayed second-order correlation function is evaluated as

$$g^{(2)}(0) = \langle\Psi(0)|c_{\rm cw}^{\dagger}c_{\rm cw}^{\dagger}c_{\rm cw}c_{\rm cw}|\Psi(0)\rangle/I_c^2 \approx \left|C_{002}^{2}\right|^2/I_c^2. \tag{D23}$$

[1] M. O. Scully and M. S. Zubairy, *Quantum Optics* (Cambridge University Press, Cambridge, 1999).

[2] J.-B. You, X. Xiong, P. Bai, Z.-K. Zhou, R.-M. Ma, W.-L. Yang, Y.-K. Lu, Y.-F. Xiao, C. E. Png, F. J. Garcia-Vidal, C.-W. Qiu, and L. Wu, Reconfigurable photon sources based on quantum plexcitonic systems, Nano Lett. **20**, 4645 (2020).

[3] J. P. Vasco, D. Gerace, P. S. S. Guimarães, and M. F. Santos, Steady-state entanglement between distant quantum dots in photonic crystal dimers, Phys. Rev. B **94**, 165302 (2016).

[4] N. Iliopoulos, I. Thanopulos, V. Yannopapas, and E. Paspalakis, Counter-rotating effects and entanglement dynamics in strongly coupled quantum-emitter–metallic-nanoparticle structures, Phys. Rev. B **97**, 115402 (2018).

[5] E. Zubizarreta Casalengua, J. C. López Carreño, F. P. Laussy, and E. d. Valle, Conventional and unconventional photon statistics, Laser Photonics Rev. **14**, 1900279 (2020).

[6] Y.-W. Lu, J.-F. Liu, Z. Liao, and X.-H. Wang, Plasmonic-photonic cavity for high-efficiency single-photon blockade, Sci. China Phys. Mech. Astron. **64**, 274212 (2021).

[7] M. Chen, J. Tang, L. Tang, H. Wu, and K. Xia, Photon blockade and single-photon generation with multiple quantum emitters, Phys. Rev. Res. **4**, 033083 (2022).

[8] J. S. Douglas, H. Habibian, C. L. Hung, A. V. Gorshkov, H. J. Kimble, and D. E. Chang, Quantum many-body models with cold atoms coupled to photonic crystals, Nat. Photonics **9**, 326 (2015).

[9] A. Chiesa, P. Santini, D. Gerace, and S. Carretta, Long-lasting hybrid quantum information processing in a cavity-protection regime, Phys. Rev. B **93**, 094432 (2016).

[10] R. Schilling, C. Xiong, S. Kamlapurkar, A. Falk, N. Marchack, S. Bedell, R. Haight, C. Scerbo, H. Paik, and J. S. Orcutt, Ultrahigh-q on-chip silicon–germanium microresonators, Optica **9**, 284 (2022).

[11] D. W. Vernooy, V. S. Ilchenko, H. Mabuchi, E. W. Streed, and H. J. Kimble, High-q measurements of fused-silica microspheres in the near infrared, Opt. Lett. **23**, 247 (1998).

[12] H. Choi, M. Heuck, and D. Englund, Self-Similar Nanocavity Design with Ultrasmall Mode Volume for Single-Photon Nonlinearities, Phys. Rev. Lett. **118**, 223605 (2017).

[13] S. Hu, M. Khater, R. Salas-Montiel, E. Kratschmer, S. Engelmann, W. M. J. Green, and S. M. Weiss, Experimental realization of deep-subwavelength confinement in dielectric optical resonators, Sci. Adv. **4**, eaat2355 (2018).

[14] S. Hu and S. M. Weiss, Design of photonic crystal cavities for extreme light concentration, ACS Photonics **3**, 1647 (2016).

[15] M.-A. Miri and A. Alù, Exceptional points in optics and photonics, Science **363**, eaar7709 (2019).

[16] R. El-Ganainy, K. G. Makris, M. Khajavikhan, Z. H. Musslimani, S. Rotter, and D. N. Christodoulides, Non-Hermitian physics and PT symmetry, Nat. Phys. **14**, 11 (2018).

[17] H.-Z. Chen, T. Liu, H.-Y. Luan, R.-J. Liu, X.-Y. Wang, X.-F. Zhu, Y.-B. Li, Z.-M. Gu, S.-J. Liang, H. Gao, L. Lu, L. Ge, S. Zhang, J. Zhu, and R.-M. Ma, Revealing the missing dimension at an exceptional point, Nat. Phys. **16**, 571 (2020).

[18] A. Pick, B. Zhen, O. D. Miller, C. W. Hsu, F. Hernandez, A. W. Rodriguez, M. Soljacic, and S. G. Johnson, General theory of spontaneous emission near exceptional points, Opt. Express **25**, 12325 (2017).

[19] W. D. Heiss, Time behaviour near to spectral singularities, Eur. Phys. J. D **60**, 257 (2010).

[20] B. Peng, S. K. Ozdemir, M. Liertzer, W. Chen, J. Kramer, H. Yilmaz, J. Wiersig, S. Rotter, and L. Yang, Chiral modes and directional lasing at exceptional points, Proc. Natl. Acad. Sci. U.S.A. **113**, 6845 (2016).

[21] J. Wiersig, Enhancing the Sensitivity of Frequency and Energy Splitting Detection by Using Exceptional Points: Application to Microcavity Sensors for Single-Particle Detection, Phys. Rev. Lett. **112**, 203901 (2014).

[22] J. Ren, S. Franke, and S. Hughes, Quasinormal mode theory of chiral power flow from linearly polarized dipole emitters coupled to index-modulated microring resonators close to an exceptional point, ACS Photonics **9**, 1315 (2022).

[23] Q. Zhong, A. Hashemi, S. K. Özdemir, and R. El-Ganainy, Control of spontaneous emission dynamics in microcavities with chiral exceptional surfaces, Phys. Rev. Res. **3**, 013220 (2021).

[24] L. Ferrier, P. Bouteyre, A. Pick, S. Cueff, N. H. M. Dang, C. Diederichs, A. Belarouci, T. Benyattou, J. X. Zhao, R. Su, J. Xing, Q. Xiong, and H. S. Nguyen, Unveiling the Enhancement of Spontaneous Emission at Exceptional Points, Phys. Rev. Lett. **129**, 083602 (2022).

[25] A. Pick, Z. Lin, W. Jin, and A. W. Rodriguez, Enhanced nonlinear frequency conversion and Purcell enhancement at exceptional points, Phys. Rev. B **96**, 224303 (2017).

[26] L. Leonforte, A. Carollo, and F. Ciccarello, Vacancy-Like Dressed States in Topological Waveguide QED, Phys. Rev. Lett. **126**, 063601 (2021).

[27] D. C. Marinica, A. G. Borisov, and S. V. Shabanov, Bound States in the Continuum in Photonics, Phys. Rev. Lett. **100**, 183902 (2008).

[28] M. Cotrufo and A. Alù, Excitation of single-photon embedded eigenstates in coupled cavity–atom systems, Optica **6**, 799 (2019).

[29] C. W. Hsu, B. Zhen, A. D. Stone, J. D. Joannopoulos, and M. Soljačií, Bound states in the continuum, Nat. Rev. Mater. **1**, 16048 (2016).

[30] H. M. Doeleman, E. Verhagen, and A. F. Koenderink, Antenna–cavity hybrids: Matching polar opposites for Purcell enhancements at any linewidth, ACS Photonics **3**, 1943 (2016).

[31] Y.-W. Lu, W. Li, R. Liu, Y. Wu, H. Tan, Y. Li, and J.-F. Liu, Plasmon-assisted low-threshold nanolasers, Phys. Rev. B **106**, 115434 (2022).

[32] M. Y. Odoi, N. I. Hammer, K. T. Early, K. D. McCarthy, R. Tangirala, T. Emrick, and M. D. Barnes, Fluorescence lifetimes and correlated photon statistics from single CdSe/oligo(phenylene vinylene) composite nanostructures, Nano Lett. **7**, 2769 (2007).

[33] M. D. Leistikow, J. Johansen, A. J. Kettelarij, P. Lodahl, and W. L. Vos, Size-dependent oscillator strength and quantum efficiency of CdSe quantum dots controlled via the local density of states, Phys. Rev. B **79**, 045301 (2009).

[34] H. J. Carmichael, Quantum Trajectory Theory for Cascaded Open Systems, Phys. Rev. Lett. **70**, 2273 (1993).

[35] W.-K. Mok, D. Aghamalyan, J.-B. You, T. Haug, W. Zhang, C. E. Png, and L.-C. Kwek, Long-distance dissipation-assisted transport of entangled states via a chiral waveguide, Phys. Rev. Res. **2**, 013369 (2020).

[36] C. Van Vlack, P. T. Kristensen, and S. Hughes, Spontaneous emission spectra and quantum light-matter interactions from a strongly coupled quantum dot metal-nanoparticle system, Phys. Rev. B **85**, 075303 (2012).

[37] K. Srinivasan and O. Painter, Mode coupling and cavity-quantum-dot interactions in a fiber-coupled microdisk cavity, Phys. Rev. A **75**, 023814 (2007).

[38] D. Tamascelli, A. Smirne, S. F. Huelga, and M. B. Plenio, Nonperturbative Treatment of Non-Markovian Dynamics of Open Quantum Systems, Phys. Rev. Lett. **120**, 030402 (2018).

[39] E. V. Denning, J. Iles-Smith, and J. Mork, Quantum light-matter interaction and controlled phonon scattering in a photonic Fano cavity, Phys. Rev. B **100**, 214306 (2019).

[40] W. K. Wootters, Entanglement of Formation of an Arbitrary State of Two Qubits, Phys. Rev. Lett. **80**, 2245 (1998).

[41] J. Hakami and M. S. Zubairy, Nanoshell-mediated robust entanglement between coupled quantum dots, Phys. Rev. A **93**, 022320 (2016).

[42] Y.-W. Lu, W.-J. Zhou, Y. Li, R. Li, J.-F. Liu, L. Wu, and H. Tan, Unveiling atom-photon quasi-bound states in hybrid plasmonic-photonic cavity, Nanophotonics **11**, 3307 (2022).

[43] P. Hu, J. Wang, Q. Jiang, J. Wang, L. Shi, D. Han, Z. Q. Zhang, C. T. Chan, and J. Zi, Global phase diagram of bound states in the continuum, Optica **9**, 1353 (2022).

[44] F. Roccati, S. Lorenzo, G. Calajò, G. M. Palma, A. Carollo, and F. Ciccarello, Exotic interactions mediated by a non-Hermitian photonic bath, Optica **9**, 565 (2022).

[45] Z. Liu, J. Wang, B. Chen, Y. Wei, W. Liu, and J. Liu, Giant enhancement of continuous wave second harmonic generation from few-layer GaSe coupled to high-q quasi bound states in the continuum, Nano Lett. **21**, 7405 (2021).

[46] H. Friedrich and D. Wintgen, Interfering resonances and bound states in the continuum, Phys. Rev. A **32**, 3231 (1985).

[47] J. Tang, L. Tang, H. Wu, Y. Wu, H. Sun, H. Zhang, T. Li, Y. Lu, M. Xiao, and K. Xia, Towards On-Demand Heralded Single-Photon Sources via Photon Blockade, Phys. Rev. Appl. **15**, 064020 (2021).

[48] J.-K. Xie, S.-L. Ma, and F.-L. Li, Quantum-interference-enhanced magnon blockade in an yttrium-iron-garnet sphere coupled to superconducting circuits, Phys. Rev. A **101**, 042331 (2020).

[49] J. R. Johansson, P. D. Nation, and F. Nori, Qutip 2: A python framework for the dynamics of open quantum systems, Comput. Phys. Commun. **184**, 1234 (2013).